Application Note

Cancer Biology

Agilent

Trusted Answers

Automated Monitoring of Protein Expression and Metastatic Cell Migration Using 3D-Bioprinted Colorectal Cancer Cells

Authors

Brad Larson and Leonie Rieger
Agilent Technologies, Inc.
Winooski, VT, USA

Glauco Souza and
Hubert Tseng
Nano3D Biosciences, Inc.
Houston, TX, USA

Arun Kumar
Enzo Life Sciences
Farmingdale, NY, USA

Introduction

Colorectal cancer (CRC) is one of the most common cancer types in the U.S., with the National Cancer Institute estimating almost 1.2 million people nationwide living with the disease as of 2013, and over 134,000 new cases expected in 2016.[1] For patients with advanced stages of CRC, there is a meager survival rate due to the cancer's predisposition to metastasize and resist treatment therapies. Previous studies have shown that the two complexes of the serine/threonine kinase mammalian target of rapamycin (mTOR), mTORC1 (containing RAPTOR) and mTORC2 (containing RICTOR) are overexpressed in CRC and play a role in tumorigenesis and metastasis.[2,3] Furthermore, upregulation of the mTOR signaling pathway has also been shown to induce expression of matrix metalloproteinases (MMPs), which also play a role in CRC metastagenicity.[4] Therefore, development of therapies that incorporate mTOR inhibitors may reduce the metastatic potential of this cancer and improve survival rates.

As colorectal cancers are solid tumors that grow *in vivo* in a three-dimensional (3D) configuration, a major limitation in the vast number of studies involving CRC research is the use of cells cultured onto a two-dimensional (2D) surface. Furthermore, cell metastatic behavior is often studied *in vitro* using phenotypic cell migration and target-based mechanism of action models. Specifically to the presented study, mTOR signaling is known to play a role in cell migration and ECM formation, which also leads to downstream expression of MMPs. The use of a 2D solid surface environment common to traditional labware results in altered cellular morphologies and behavior, as well as a lack of complex cell-cell or cell-extracellular matrix (ECM) interaction networks which often influences cell function, ECM production, and cell migration. 3D cell cultures remedy these shortcomings by providing a method that enables cells to reorganize and migrate into a structure that better replicates an *in vivo* microenvironment by capturing cell-cell and cell-ECM interactions. This development provides an improved predictive *in vitro* model for cancer metastasis.

This application note demonstrates a magnetic 3D bioprinting cell culture platform (Figure 1), where cells are first incubated with a biocompatible magnetic nanoparticle assembly consisting of gold, iron oxide, and poly-L-lysine, which magnetizes the cells without eliciting deleterious biological effect. The cells are then placed into a microplate well and levitated by placing a magnet above the well, where they aggregate and form ECM within a few hours. After this initial levitation step, the magnet is removed, and the 3D aggregates are dissociated into a disperse cell suspension of single cells and small cell aggregates by gentle pipetting action. Cells are then transferred to a 384-well assay plate and a spheroid magnet is positioned below the plate for an appropriate incubation period, allowing the cells within each well to be patterned into a dot or spheroid configuration depending upon the experiment being performed. Moreover, the magnetized spheroid can be held intact while exchanging liquids to improve sample retention, such as during regular media exchanges.

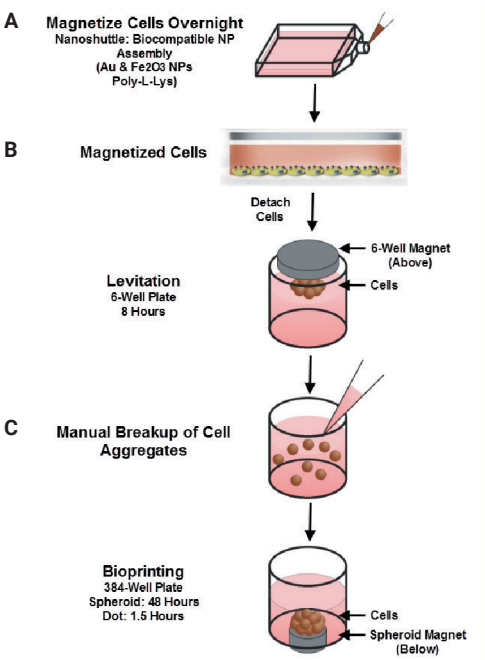

Figure 1. BiO assay kit protocol. The 384-well BiO assay kit uses the NanoShuttle-PL nanoparticle assembly to (A) magnetize cells. After incubation (B), cells are detached, resuspended in a cell-repellent plate, and magnetically levitated to aggregate and induce ECM. After breaking up the aggregates (C), single cells are transferred to a 384-well cell-repellent plate placed atop a 384-well magnet, where they aggregate at the well bottom.

Following removal of the magnet, protein expression within spheroid models was quantified via immunofluorescence, while rates of phenotypic cell migration were assessed using kinetic live cell brightfield imaging to track cell and ECM movement away from the original pattern. Mechanism of action and tumorigenesis were also determined by microplate reading and fluorescent imaging, respectively. Normal and cancerous co-cultured colon cell models were incorporated to test protein expression, whereas cell migration was analyzed using HCT116 colorectal cancer cells only. Automated imaging and microplate reading were performed using a novel cell imaging multimode reader. The combination of 3D cell model and image-based analysis provides easy-to-use, robust methods to quantify protein expression and 3D cell migration allowing confirmation of the role that mTOR signaling plays in the development and treatment of colorectal cancer.

Materials and methods

Materials

Cells

HCT116 epithelial colorectal carcinoma cells (part number CCL-247) and CCD 841 CoN colon epithelial cells (part number CRL-1790) were obtained from ATCC (Manassas, VA). RFP expressing human neonatal dermal fibroblasts (part number cAP-0008RFP) were obtained from Angio-Proteomie (Boston, MA).

Antibodies and inhibitor compounds

Rabbit antihuman mTOR polyclonal antibody (part number ADI-905-687), mouse antihuman raptor monoclonal antibody (10E10) (part number ADI-905-765), mouse antihuman rictor monoclonal antibody (1G11) (part number ADI-905-766), goat antimouse IgG1 (ATTO 590 conjugate) (part number ALX-211-204TM-C100), and goat antimouse IgG (ATTO 647N conjugate) (part number ALX-211-205); and inhibitor compounds rapamycin (part number BML-A275), KU-0063794 (part number ENZ-CHM135) and oxaliplatin (part number ALX-400-042) were generously donated by Enzo Life Sciences (Farmingdale, NY). Donkey antirabbit IgG H&L (Alexa Fluor 647) polyclonal antibody (part number ab150075) was obtained by Abcam (Cambridge, MA).

Assay and experimental components

The 384-well BiO assay kit (GBO part number 781846, consisting of 2 vials NanoShuttle-PL, 6-well levitating magnet drive, 384-well spheroid and holding magnet drives (2), 96-well deep well mixing plate, 6-well and 384-well clear cell-repellent surface microplates), prototype 384-well ring drive and additional cell-repellent surface 6-well (GBO part number 657860) and 384-well black µClear microplates (GBO part number 781976), were generously donated by Nano3D Biosciences, Inc. (Houston, TX) and Greiner Bio-One, Inc. (Monroe, NC). Matrix metalloproteinase-9 (MMP-9) fluorometric drug discovery kit (part number BML-AK411), and chemiluminescent ApoSENSOR cell viability assay kit (part number ALX-850-247) were donated by Enzo Life Sciences (Farmingdale, NY).

Agilent BioTek Cytation 5 cell imaging multimode reader

Cytation 5 is a modular multimode microplate reader combined with automated digital microscopy. Filter- and monochromator-based microplate reading are available, along with laser-based excitation for Alpha assays. The microscopy module provides up to 60x magnification in fluorescence, brightfield, color brightfield, and phase contrast. With special emphasis on live cell assays, Cytation 5 features shaking, temperature control to 65 °C, CO_2/O_2 gas control, and dual injectors for kinetic assays. The instrument performed kinetic imaging of the 3D cell structure using brightfield and multiple fluorescent imaging channels. Integrated Agilent BioTek Gen5 microplate reader and imager software controls Cytation 5, and also automates image capture, analysis and processing.

Methods

Cell preparation

T-75 flasks of HCT116, human colon, or fibroblast cell cultures were cultured to 80% confluence, then treated with 600 µL NanoShuttle-PL overnight at 37 °C/5% CO_2. After incubation, cells were trypsinized, washed, and incubated for three to five minutes at 37 °C/5% CO_2. Cells were removed from the flasks and added to the 6-well cell-repellent plate at a concentration of 1.2×10^6 cells/well. A 6-well magnet drive was placed atop the well plate to levitate the cells, where they aggregated into 3D structures and induced ECM formation during an eight-hour incubation at 37 °C/5% CO_2. After incubation, the cells and ECM were broken up, resuspended, and added to 384-well cell-repellent plate wells. For protein expression experiments, cells were resuspended at a total concentration of 2.0×10^5 cells/mL, and a total of 10,000 cells were dispensed in a volume of 50 µL. Tests involving co-cultured fibroblasts and colon cells included combining cell types in a 1:1 ratio so that 10,000 total cells were dispensed in the 50 µL volume. For cell migration experiments, cells were resuspended at a total concentration of 2.22×10^5 cells/mL, and a total of 10,000 cells were dispensed in a volume of 45 µL. A 384-well spheroid magnet drive was placed below the test plates, and the assembly was incubated at 37 °C/5% CO_2 for 48 hours to allow cells within each well to aggregate into spheroids for protein expression assessment. Assembly incubation totaled 1.5 hours for migration tests to create an epithelial layer-like dot configuration of cells and ECM.

Following completion of the aggregation process, protein expression plates were removed from the spheroid magnet drive. Migration plates remained on the spheroid drive where 5 µL of 10x titrations of rapamycin or KU-0063794 were added to the wells before removal of the plate from the magnet drive.

Protein expression assay procedure

Immunofluorescent staining was performed with HCT116/fibroblast and normal colon/fibroblast co-culture spheroid models using the procedure outlined in Table 1. Expression of mTOR, RAPTOR, and RICTOR protein in each model was assessed using the specific primary and secondary antibodies detailed in Table 2.

Following completion of the immunostaining procedure, the plate was imaged by the Agilent BioTek Cytation 5 using a 10x objective, 2 × 2 image montage, and the brightfield channel to image all cells, RFP channel to image fibroblasts, and either the CY5 channel to capture the Alexa Fluor 647 and ATTO 647N signal or the Texas Red channel to capture the ATTO 590 signal.

Cell migration assay procedure

384-well microplates were placed into Cytation 5 where automated brightfield imaging was performed every 30 minutes over a 48-hour incubation period. A 2.5x objective was used to capture single images from each test well.

Cell viability

ApoSENSOR assay components were prepared according to manufacturer protocols. The 384-well microplate was placed on the holding magnet drive and media removed via pipetting. 50 µL of nuclear releasing reagent was then added followed by mixing by pipette and a 5-minute incubation at RT. 5 µL of ATP monitoring enzyme was then added to the wells, and the microplate was placed into an Agilent BioTek Cytation 5 where the luminescent signal from each well was measured.

MMP-9 activity

The 400 µM DMSO stock of OmniMMP fluorogenic substrate peptide was thawed and diluted 1:10 in cell media. Test compounds and the no compound control were diluted in the media plus 40 µM substrate. 5 µL volumes were then added to the existing 45 µL and the microplate placed into an Agilent BioTek Cytation 5. Fluorescent signal from the cleaved substrate was measured by setting the monochromators to an excitation wavelength of 328 nm and an emission wavelength of 420 nm along with a 20 nm bandwidth. Readings were taken at the same intervals previously described for the cell migration assay procedure.

Table 1. Spheroid fixing and staining procedure.

Number	Step	Explanation	Iteration/Incubation Time
1	Plate placement	Place microplate on holding magnet drive	
2	Wash	Aspirate media and add 50 µL PBS	Incubate 5 minutes following each addition/Repeat 2x
3	Fixation	Aspirate PBS and add 50 µL 4% paraformaldehyde	60 minutes
4	Permeabilization	Aspirate 4% paraformaldehyde and add 50 µL 0.2% Tritonx100	60 minutes
5	Wash	Aspirate media and add 50 µL PBS	
6	Blocking buffer addition	Aspirate PBS and add 50 µL 1% BSA/5% goat serum in PBS	60 minutes
7	Primary antibody preparation	Dilute primary antibody according to specifications	
8	Primary antibody addition	Aspirate PBS and add 50 µL diluted primary antibody	Overnight at 4 °C
9	Wash	Aspirate primary antibody and add 50 µL PBS	Repeat 3x
10	Secondary antibody preparation	Dilute secondary antibody according to specifications	
11	Secondary antibody addition	Aspirate PBS and add 50 µL diluted secondary antibody	5 hours at RT
12	Wash	Aspirate secondary antibody and add 50 µL PBS	Repeat 3x
13	Imaging preparation	Aspirate final wash and add 50 µL PBS	Store at 4 °C until time of imaging

Table 2. Protein primary and secondary antibodies.

Protein	Primary Antibody	Dilution	Secondary Antibody	Dilution
mTOR	Rabbit antihuman mTOR polyclonal antibody	1:100	Donkey antirabbit IgG H&L (Alexa Fluor 647) polyclonal antibody	1:200
RAPTOR	Mouse antihuman raptor monoclonal antibody (10E10)	1:100	Goat antimouse IgG1 (ATTO 590 conjugate)	1:200
RICTOR	Mouse antihuman rictor monoclonal antibody (1G11)	1:100	Goat antimouse IgG (ATTO 647N conjugate)	1:200

Results and discussion

Protein expression

Upon completion of antibody staining, fluorescent imaging was completed to capture the fluorescent signal from protein bound antibody. Brightfield and fluorescent imaging was also carried out to identify the location of both cell types within the co-cultured spheroids and RFP expressing fibroblasts, respectively (Figure 2).

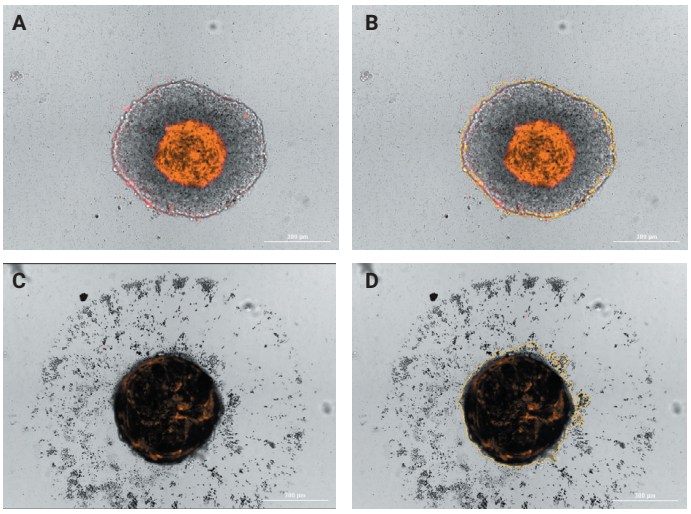

Figure 2. Detection and analysis of protein-bound immunofluorescence. (A) Brightfield, RFP, CY5 overlaid image of HCT116/RFP expressing fibroblast spheroid; (B) overlaid image plus Agilent BioTek Gen5-placed object mask around the spheroid structure; (C) brightfield, RFP, CY5 overlaid image of normal colon/RFP-expressing fibroblast spheroid; (D) overlaid image plus Gen5-placed object mask around spheroid structure.

Initial observation of overlaid brightfield, RFP, and CY5 images revealed variances in cellular organization between colon epithelial cells and fibroblasts in normal and diseased spheroidal models. HCT116 cells and fibroblasts organize in a mutually exclusive manner where the cancer cell line layers on top of a fibroblast core (Figure 2A). Conversely, normal colon cells and fibroblasts organize in an inclusive way that promotes even distribution of each cell type within the spheroid (Figure 2C).

Protein expression was then determined within each spheroid. Object masks were placed around the spheroidal object using the change in contrast in the brightfield signal between cellular and background areas. The object mask allowed quantification of all immunofluorescence solely within the spheroid area using the "Object Int" calculated metric. Integrated CY5 fluorescence from test spheroids for each co-cultured cell model was then tabulated.

Figure 3 illustrates that mTOR, RAPTOR, and RICTOR protein expression was increased by as much as eight-fold in diseased colon epithelial cell spheroid models compared to normal colon cell spheroids. This confirms previously published findings that expression of mTOR and its components RAPTOR and RICTOR are greatly increased in colorectal cancers[3], and suggests that the 3D co-cultured HCT116/fibroblast spheroidal model is a suitable surrogate to perform *in vitro* testing.

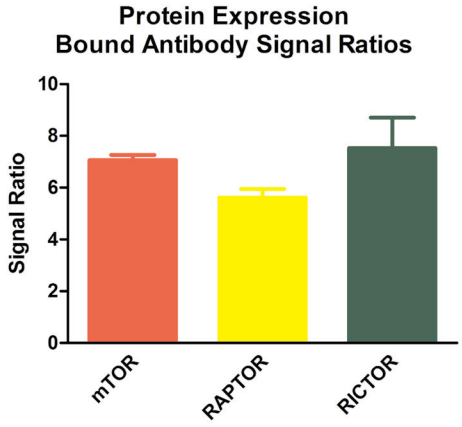

Figure 3. Protein expression quantification. Fluorescent signal from labeled secondary antibodies bound to primary antibodies specific for mTOR, RAPTOR, or RICTOR proteins. The signal ratio was calculated by comparing the signal from HCT116 cells/fibroblasts to normal colon cells/fibroblasts.

Cell migration

The ability of bioprinted cells to demonstrate metastatic behavior by means of cell migration, as well as the image-based monitoring and analysis to properly quantify the migration was then examined. Using the parameters in Table 3, the images were preprocessed to improve appropriate placement of object masks around the complete migrating structure during the cellular analysis step. As observed when comparing Figures 4A and 4B, the change in intensity from the middle of the brightfield image to the outer edge is removed, or flattened providing an image of satisfactory contrast where the cellular aggregate is much easier to analyze.

Table 3. Brightfield image preprocessing parameters.

Parameter	Description
Image Set	Brightfield
Background	Light
Rolling Ball Diameter	300 µm
Image Smoothing Strength	3 cycles of 3 × 3 average filter

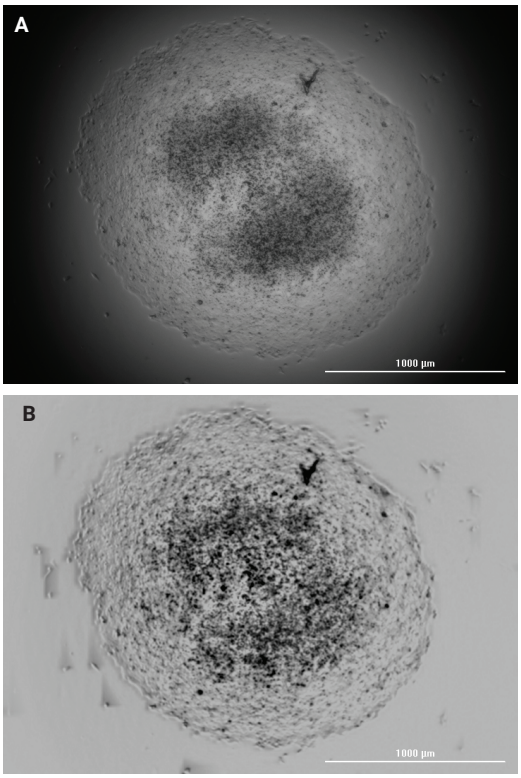

Figure 4. Image background signal removal via preprocessing. Representative brightfield image, using a 2.5x objective (A) before; and (B) after preprocessing.

Upon examination of the kinetic brightfield images of uninhibited cell and ECM migration in Figure 5, captured using the parameters previously explained, it can be seen that both cells and matrix move away from the original printed area over time to cover an increasing portion of the well. Migration is then completely inhibited by 10 µM concentrations of rapamycin or KU-0063794, compounds known to inhibit cell signaling pathways leading to mTOR activation.

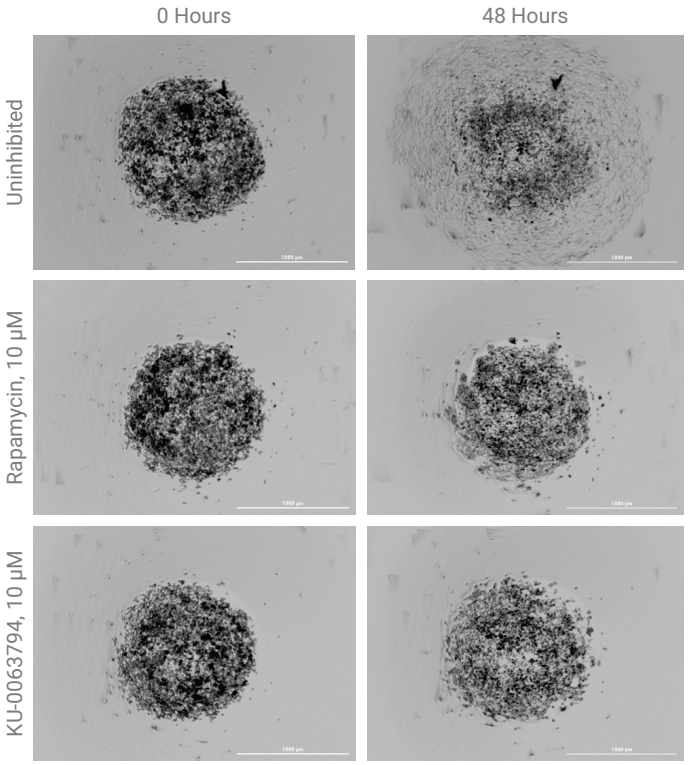

Figure 5. HCT116 cell migration over a 48-hour incubation. Brightfield images, using a 2.5x objective, captured from individual wells of HCT116 cells treated and incubated as follows: (Row 1) untreated, 0 to 48 hours; (Row 2) 10 µM rapamycin, 0 to 48 hours; (Row 3) 10 µM KU-0063794, 0 to 48 hours.

Once all images were preprocessed, detailed object masks using the change in brightfield signal, as well as other parameters detailed in Table 4, were automatically and accurately placed around the migrating 3D structure composed of cells and ECM as demonstrated in Figure 6.

Table 4. Brightfield image object masks parameters.

Cell Migration Cellular Analysis Parameters	
Imaging Channel	Brightfield
Threshold	500
Background	Light
Split Touching Objects	Unchecked
Fill Holes in Masks	Checked
Minimum Object Size	500 µm
Maximum Object Size	2,500 µm
Include Primary Edge Objects	Checked
Analyze Entire Image	Checked
Advanced Analysis Parameters	
Rolling Ball Diameter	100 µm
Image Smoothing Strength	5 cycles of 3 × 3 average filter
Evaluate Background On	20% of lowest pixels

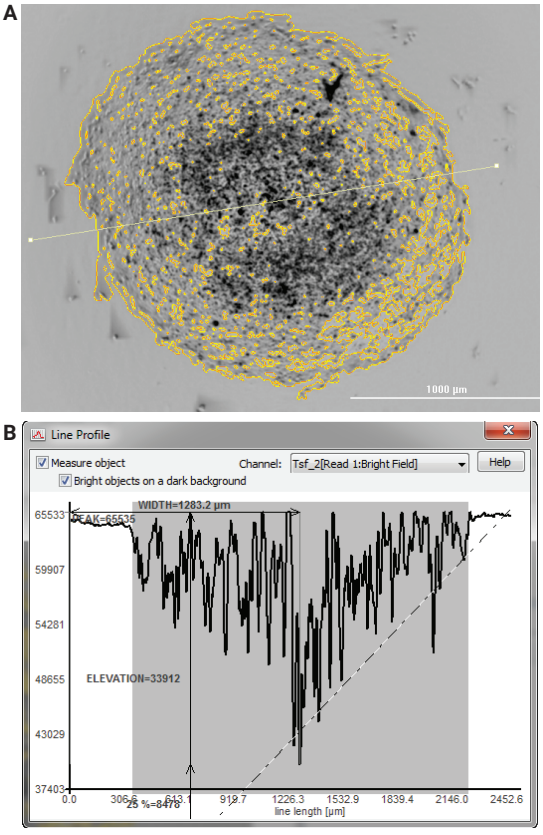

Figure 6. Cellular analysis. (A) Preprocessed brightfield image, using a 2.5x objective, with object mask automatically placed around cells and ECM using Agilent BioTek Gen5 microplate reader and imager software. A line was drawn through the background, cell, and ECM-containing portions of the image using the Line Profile Tool. (B) A graph of the brightfield signal along all portions of the drawn line representing signal change used by Gen5 to automatically construct the object mask.

Area within each 3D structure was automatically returned by Gen5 as a calculated metric at each time point for the 0 to 10,000 nM concentrations of rapamycin and KU-0063794 tested. Then fold change values were calculated by the following formula and graphed (Figure 7).

$$Area_{time\ X}/Area_{time\ 0}$$

Figure 7 demonstrates that both rapamycin and KU-0063794 have a dose-dependent effect on the migratory ability of HCT116 cells. The results also confirm published findings that inhibition of mTOR signaling attenuates migration of CRCs.[3] A more complete inhibitory effect is seen from KU-0063794 at the 10 µM concentration compared to rapamycin. This may be due to the fact that rapamycin inhibits only mTORC1 in an acute manner, but has little effect on mTORC2[5], whereas KU-0063794 is a known inhibitor of both mTOR complexes.[6]

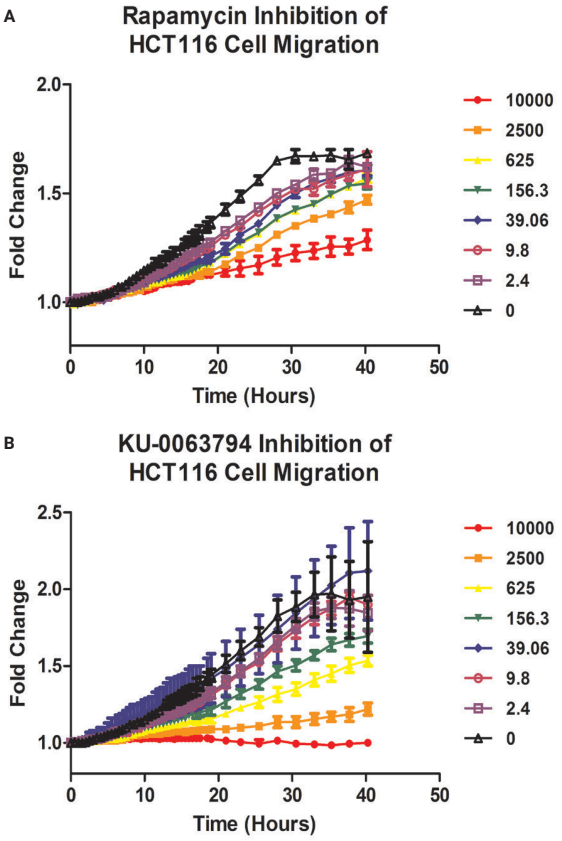

Figure 7. Kinetic HCT116 cell migration analysis. Area fold change of cells exposed to 0 to 10,000 nM (A.) rapamycin; or (B) KU-0063794 compared to coverage area at time 0.

Relative cell viability was also measured pre- and postincubation to assess whether the change in cell and ECM coverage area was due to actual cell migration or to cell proliferation. ApoSENSOR reagent, which measures cellular ATP levels, was added to wells containing untreated HCT116 cells and matrix, incubated at hours 0 and 48, following the manufacturer's protocol. Luminescent signal from test wells was captured and quantified using an Agilent BioTek Cytation 5. Statistical analysis (data not shown), using a t-test on luminescence data generated before and after the 48-hour incubation period, revealed no significant change between the two data sets with greater than 99% confidence. This confirms that the change in cell/ECM coverage area is not due to cell proliferation, but rather due to existing cell migration.

Matrix metalloproteinase mechanism of action

Matrix metalloproteinase (MMP) production, which is regulated by the mTOR signaling pathway, is shown to play a role in the invasive and migratory ability of CRCs. MMPs are typically active at the leading edge of invasive structures where they degrade ECM proteins and facilitate the first part of the metastatic process.

With the addition of the live cell fluorogenic MMP-9 substrate to each test well at time 0, it could be determined if inhibition of the mTOR signaling pathway by rapamycin or KU-0063794 not only played a role in the interruption of phenotypic cell migration, but also in MMP-9 production.

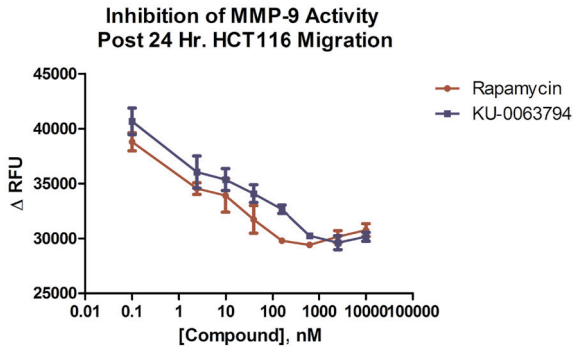

Figure 8. Detection of MMP-9 activity. Plot of ΔRFU values upon cleavage of fluorogenic MMP-9 substrate after 0 and 24 hours incubations from wells treated with rapamycin or KU-0063794. Fluorescent signal captured using an Agilent BioTek Cytation 5 cell imaging multimode reader with monochromator settings of Ex 328 and Em 420 with a 20 nm bandwidth.

Increases in MMP-9 activity, as indicated by increasing fluorescence values from test wells, stabilized after 24 hours of incubation. The change in fluorescence from RFU values recorded at time 0 for each individual well at this time point were then plotted in the graph seen in Figure 8. By observing the results, it can be seen that ΔRFU values decrease with increasing concentrations of rapamycin and KU-0063794, indicating a dose-dependent inhibitory effect on MMP-9 enzyme activity. These data validate results previously reported, that knock-down of RAPTOR and RICTOR proteins decreases levels of MMP-9 secretion.[3]

Conclusion

The 384-well BiO assay kit and NanoShuttle-PL particles manufactured by nano3D Biosciences provide a simple, robust method to create biomimetic, ECM-including structures that resemble a primary tumor. This facilitates the accurate assessment of changes in protein expression between normal and diseased 3D cell models, and the effect that inhibiting cell signaling pathways have on metastatic cell migration. The CRC model chosen in this application note has demonstrated that mTOR and its protein complexes involving RAPTOR and RICTOR are highly overexpressed relative to undiseased co-cultured cells. This is linked to significant cell migration in the 3D-bioprinted model used that is aided by matrix metalloproteinase production. Using known inhibitors of mTOR protein complexes, cell migration can be impeded or completely stopped over the time course of the experiments. This is in part due to reduction of matrix metalloproteinase activity.

References

1. National Cancer Institute Surveillance, Epidemiology, and End Results Program. https://seer.cancer.gov/statfacts/html/colorect.html (accessed Aug 5, 2016).
2. Gulhati, P. *et al.* Targeted Inhibition of mTOR Signaling Inhibits Tumorigenesis of Colorectal Cancer. *Clin. Cancer Res.* **2009**, *15(23)*, 7207–7216.
3. Gulhati, P. *et al.* mTORC1 and mTORC2 Regulate EMT, Motility and Metastasis of Colorectal Cancer via RhoA and Rac1 Signaling Pathways. *Cancer Res.* **2011**, *71(9)*, 3246–3256.
4. Wang, G. *et al.* APRIL Induces Tumorigenesis and Metastasis of Colorectal Cancer Cells via Activation of the PI3K/Akt Pathway. *PLoS One [Online]* **2013**, *8(1)*. http://journals.plos.org/plosone/article?id=10.1371/journal.pone.0055298 (accessed Sep 9, 2016).
5. Schreiber, K. H. *et al.* Rapamycin-Mediated mTORC2 Inhibition is Determined by the Relative Expression of FK506-Binding Proteins. *Aging Cell* **2015**, *14(2)*, 265–273.
6. Zhang, H. *et al.* A Comparison of Ku0063794, a Dual mTORC1 and mTORC2 Inhibitor, and Temsirolimus in Preclinical Renal Cell Carcinoma Models. *PLoS One [Online]* **2013**, *8(1)*. http://journals.plos.org/plosone/article?id=10.1371/journal.pone.0054918 (accessed Sep 12, 2016).

www.agilent.com/lifesciences/biotek

RA44412.3905555556

Printed in the USA, April 20, 2022
5994-3376EN

Agilent
Trusted Answers